Modelling the hygrothermal behaviour of cement-bonded wood composite panels as permanent formwork

M. Li, V. Nicolas, M. Khelifa, M. El Ganaoui, V. Fierro, A. Celzard

Modelling the hygrothermal behaviour of cement-bonded wood composite panels as permanent formwork

M. Li[1,3], V. Nicolas[4,*], M. Khelifa[1], M. El Ganaoui[2], V. Fierro[4], A. Celzard[4]

[1]*Université de Lorraine, LERMAB, EA 4370, 27 rue Philippe Séguin, 88000 Epinal, France*
[2]*Université de Lorraine, LERMAB, EA 4370, 186 rue de Lorraine, 54400 Cosnes-et-Romain, France*
[3]*Université de Cergy-Pontoise, L2MGC, EA 4114, 5 mail Gay-Lussac, 95031 Neuville-sur-Oise, France*
[4]*Université de Lorraine, CNRS, IJL, 88000 Epinal, France*

[*] Corresponding author. Tel: + 33 372 74 96 54. Fax: + 33 372 74 96 38. E-mail address : vincent.nicolas@univ-lorraine.fr (V. Nicolas)

Keywords: Wood-cement composite; Heat and moisture transfer; Hygrothermal behaviour; Numerical model; Moisture buffering value.

Abstract

This paper reports on the hygrothermal behaviour of a new bio-based composite building material, based on recycled wood fibres used as eco-aggregate within a cementitious matrix. A coupled heat and moisture transfer was established through the material and resolved numerically with a model developed herein. Relative humidity and temperature were chosen as driving potentials. The hygric and thermal properties of the material were analysed and then used as input parameters in the model. The accuracy of the latter was verified by comparing the simulation results with experimental hygrothermal tests, from which the moisture buffering value (MBV) could be determined. The MBV showed that the wood-cement composite material might contribute to improve the indoor thermal comfort and be relevant for low-energy building design.

Abbreviations

1) EN197/1: European standard of Cement- Part 1: Composition, specification and conformity criteria for common cements

2) ISO12571-2000: Hygrothermal performance of building materials and products: Determination of hygroscopic sorption properties, 2000.

3) ASTM C1498-01: Standard Test Method for Hygroscopic Sorption Isotherms of Building Materials, ASTM International, West Conshohocken, PA, 2001

Nomenclature

Letters

A	area, m^2
c_p	specific heat, $J.kg^{-1}.K^{-1}$
D_θ	moisture diffusivity, $m^2.s^{-1}$
D_T	moisture diffusivity associated to a temperature gradient, $m^2.s^{-1}.K^{-1}$
e	thickness, m
$\dot{g}$	moisture diffusion flux, $kg.m^{-2}.s^{-1}$
h_{surf}	global heat transfer coefficient, $W.m^{-2}.K^{-1}$
h_c	convective heat transfer coefficient, $W.m^{-2}.K^{-1}$
h_r	radiative heat transfer coefficient, $W.m^{-2}.K^{-1}$
$\dot{H}$	total volumetric enthalpy, $J.m^{-3}$
L_v	latent heat of vaporisation, $J.kg^{-1}$
m	mass, g
P_v	partial pressure of water vapour, Pa
$P_{v,sat}$	saturated water vapour pressure, Pa
$\dot{q}$	heat flux, $W.m^{-2}$
φ_a	ambient relative humidity, %
t	time, s

T	temperature, K
U	moisture content, $kg.kg_s^{-1}$

Greek symbols

β_m	convective moisture transfer coefficient, $m.s^{-1}$
θ	moisture volumetric content, $kg.m^{-3}$
λ	thermal conductivity, $W.m^{-1}.K^{-1}$
φ	relative humidity, %

Subscripts

a	air
l	liquid
ref	reference
s	dry material
surf	upper material surface
v	vapour

1 Introduction

Wood-cement composite panels have been invented quite a long time ago, and the interest for such materials was renewed in the 1960's due to the restricted use of asbestos (Campbell and Coutts, 1980). Their main benefit is related to the availability of natural raw materials and to their reduced environmental impact, compared to many synthetic materials. Pervaiz and Sain, (2003) indeed proved that wood-based composites can behave as a 'sink' to store carbon dioxide. Another study confirmed that 1 m^2 of plant-based concrete wall can store 14 to 35 kg of carbon dioxide for over 100 years (Boutin et al., 2006). In addition, the presence of wood fibres has the advantage of improving the mechanical properties of the cementitious matrix (Akkaoui et al., 2017).

According to ADEME (French Environment & Energy Management Agency), 6.2 million tons of wood waste are produced every year in France. As any organic waste, timber biodegrading at landfill increases carbon emissions (Kim and Song, 2014), and even toxic gases can be emitted from former chemical treatments that had been used for wood preservation (Helsen and Van den Bulck, 2005). Recently, the use of wood waste as substitute to wood fibres in concrete has been highlighted by many studies as an excellent way of reducing timber disposal at landfills. Moreover, a number of works focused on recycling and reusing wood waste as aggregate in concrete or mortar, which is now becoming a sustainable and advanced solution for building materials (Lo, 2017; Sudin and Swamy, 2006; Wang et al., 2016a).

The hygrothermal performances of several vegetable fibres-filled cementitious matrices have already been studied, such as wood-cement composite (Akkaoui, 2014; Bouguerra et al., 1999), hemp-lime concrete (Dhakal et al., 2017; Evrard and deHerd, 2010; Lelievre et al., 2014; Tran Le et al., 2010), flax shives-cement (Page et al., 2017), rape straw-lime concrete

(Rahim et al., 2015), etc. These works used either experimental or numerical approaches, at different scales, to evaluate their properties. The results showed that building materials based on natural fibres offer interesting thermal and hygric properties (Cetiner and Shea, 2018), good phonic insulation, and good moisture-buffering capacity. Karade, (2010) reviewed the generation of lignocellulosic wastes (agro-forestry waste and construction demolition waste) in the world, their mechanical characteristics, as well as their advantages and limitations. Vegetable fibres added into cementitious matrices contribute to enhance fracture toughness and durability of buildings (Cheah and Ramli, 2011; Chowdhury et al., 2015; Wang et al., 2016b).

Herein, our interest focused on a new wood-cement composite panel, which can be used as an insulating stay-in-place or permanent formwork of buildings (Fig. 1). This permanent formwork system can be applied to modular construction, using a fast and simple assembly phase. The dimensions of formwork panels are as follows: length 2 m, height 0.5 m, and thickness 25, 35 or 50 mm. In addition to formwork, the system is composed of a prefabricated polystyrene insulation layer and a cast in situ concrete layer. Steel rods of diameter 3 mm contribute to the stability of the structure and to the connection of upper and lower formwork panels.

Located on both inner and outer faces of the walls, the wood-cement composite panels are exposed to many thermal and hygric stresses due to differences of temperature and humidity between opposite wall sides. The hygrothermal transfers may thus cause condensation problems, which are likely to produce mould, or at least to influence the physical properties of the walls, such as a drop of their thermally insulating character, a decrease of mechanical properties, the degradation of the interior plaster, etc., and may also induce excess energy consumption caused by ventilation needs.

120 This paper aims at characterising the hygrothermal behaviour of wood-cement composite
121 panels through experimental and numerical approaches in order to prove their positive
122 influence on the regulation of humidity, thus contributing to indoor comfort, and to promote
123 their use in construction. The present work thus investigates heat and moisture transfers in
124 such porous media based on a cementitious matrix filled with wood fibres. A numerical model
125 consisting of two nonlinear partial differential equations was established and implemented in
126 the Comsol Multiphysics software in order to describe and predict heat and moisture transfers
127 through the material. In section 2, the experimental setup is presented, whereas the
128 mathematical model is described in section 3. Then, the determination of input properties,
129 formerly absent from the literature, is detailed in section 4. Finally, the numerical model is
130 applied and validated in section 5, wherein the results are compared with those from the
131 experiments and shown to be usable for predicting the hygrothermal transfers in this kind of
132 material. The moisture buffering capacity of the composite material is also estimated, and its
133 interest in building is discussed.

134 ## 2 Materials and methods

135 ### 2.1 Material formulation

136 The present wood-cement composite panel was already investigated elsewhere in terms
137 of thermal and mechanical properties (Li et al., 2019, 2018, 2017). Its main mechanical
138 characteristics are presented in Table 1. It is based on wood shavings from spruce, considered
139 as a waste from the wood industry and used as aggregate, and on Portland cement type CEM
140 II/A-L 42.5R, according to EN197/1 [1] used as matrix. Waterglass was also part of the
141 composite formulation for improving the internal bonding between wood fibre and cement.

[1] EN-197-1 European standard of Cement- Part 1: Composition, specification and conformity criteria for common cements

142 The wood shavings were first impregnated by soaking in the sodium silicate solution for
143 24 h before being mixed with cement CEM II. The mixture was then poured into the mould
144 and gently pressed to accelerate the curing of the cement and improve the mechanical
145 properties.

146 The raw bio-aggregate and the final composite material are shown in Fig. 2. Table 2
147 indicates the proximate composition of the composite, whose dry density was evaluated at
148 750 ± 20 kg/m^3.

149 2.2 Experimental setup

150 Former works demonstrated that hygroscopic materials can regulate the indoor relative
151 humidity and hence improve the comfort felt by the occupants (Hameury and Lundström,
152 2004; Qin et al., 2009; Wang et al., 2016a). The material behaviour with respect to moisture is
153 normally measured at steady-state, but studying the hygric behaviour under dynamic
154 conditions is much more representative of the real environment. One important parameter is
155 the moisture buffering value (MBV), which quantifies the ability of hygroscopic building
156 materials to store and release moisture. The measurement method proposed in the
157 NORDTEST project (Rode, 2005) was used here, and is based on a fast cycling test repeated
158 during at least 9 days at a fixed temperature (23°C): high relative humidity (75%) during 8
159 hours, and then low relative humidity (33 %) during 16 hours.

160 Herein, a $10 \times 10 \times 3.5$ mm wood-cement composite sample was both thermally insulated
161 and isolated from moisture on all sides except one. The top side indeed remained in contact
162 with air, as shown in Fig. 3a. With such configuration, unidirectional transfer was allowed in
163 the material. The sample was placed in a temperature- and humidity-controlled climatic
164 chamber (Fig. 3), inside which a sensor was introduced to record the actual values of both
165 relative ambient humidity and temperature. The changes of mass of the sample were

166 continuously followed with an electronic balance, also installed in the climatic chamber, and
167 connected to a computer. Two Sensirion K-type thermocouples were placed at different
168 depths inside the sample (8 and 24 mm) for monitoring the temporal changes of temperature
169 (Fig. 3c).

170 Prior to the test, the sample was dried at 60°C in a ventilated oven in order to measure its
171 dry mass. Then, the sample was reconditioned at a temperature of 23°C and relative humidity
172 of 50% in a climatic chamber. After stabilisation, dynamic relative humidity conditions were
173 imposed while the temperature in the chamber was maintained at 23°C.

174 The changes of both temperature and relative humidity in the climatic chamber, recorded
175 by a sensor type "HOBO MX CO_2 logger", are shown in Fig. 4. The recorded values were
176 then used as boundary conditions for the simulation.

177 **3 Mathematical model**

178 The phenomenon of moisture transfer in any building envelope considered as a porous
179 medium is driven by the diffusion of moisture in either liquid or vapour form, or both. The
180 transfer mechanisms are not the same, depending on the phases: liquid water can be
181 transported under the effect of a capillary pressure gradient, but the transport of water vapour
182 is induced by a partial vapour pressure gradient. On the other hand, heat transfer occurs by
183 one or a combination of the following mechanisms: conduction (temperature gradient),
184 convection (air circulation), radiation (electromagnetic waves) and phase change
185 (evaporation-condensation).

186 Generally, the combined heat, air and moisture (HAM) transfers in a porous medium can
187 be described by a system of partial differential equations (Kunzel, 1995; Luikov, 1966; Qin et
188 al., 2009; Rode, 2005). Many models have been presented in the literature that can solve the
189 HAM problem by analytical methods (Qin and Zhang, 2015), or by numerical approaches

such as WUFI (Park et al., 2019; Yoo et al., 2019), Comsol Multiphysics (Colinart and Glouannec, 2017; Lelievre et al., 2014; Liu et al., 2015), Matlab (Wang and Ge, 2018), etc. Recently, Lopez et al. reviewed the codes available for HAM simulation as well as the input parameters that are needed (López et al., 2017).

The model developed in the present study is based on the theory proposed by Luikov (Luikov, 1966) and then solved with Comsol Multiphysics. In this context, the building material is assumed to be a porous but continuous and homogeneous medium, and the system is considered in thermodynamic equilibrium. Besides, the shrinkage, the radiation, and the effect of gravity are neglected. The liquid phase is assumed to be incompressible (ρ_l = constant), and the solidification of water is neglected because the average temperature in winter is usually higher than 0°C.

3.1 Leading equations

3.1.1 Moisture transfer

The phenomenon of moisture transfer in a building envelope is expressed by the mass conservation of liquid and vapour phases:

$$\frac{\partial \theta}{\partial t} + \vec{\nabla} \cdot \left(\vec{g}_l + \vec{g}_v \right) = 0 \text{ with:} \quad (1)$$

$$\vec{g}_l = -D_{l,\theta} \vec{\nabla} \theta - D_{l,T} \vec{\nabla} T = -D_{l,\theta} \xi \vec{\nabla} \varphi - D_{l,T} \vec{\nabla} T \quad \text{and} \quad (2)$$

$$\vec{g}_v = -D_{v,\theta} \vec{\nabla} \theta - D_{v,T} \vec{\nabla} T = -D_{v,\theta} \xi \vec{\nabla} \varphi - D_{v,T} \vec{\nabla} T \quad (3)$$

where θ [kg/m^3] is the volumetric moisture content, and $\vec{g}_l$ and $\vec{g}_v$ [kg/(m^2.s)] are liquid and vapour diffusion fluxes, respectively. $D_{i,\theta}$ [m^2/s] is the moisture diffusivity in each phase, the index i representing the different possible states of water: (l) for liquid and (v) for vapour. $D_{i,T}$ [m^2/(s.K)] is the moisture diffusivity associated to temperature gradient, and since it contributes to less than 0.05% of water and vapour transport (Liu et al., 2015), it was

neglected in our case, i.e., we fixed $D_{i,T}$ = 0. $\xi = \partial\theta / \partial\varphi = \rho_s \left(\partial u / \partial\varphi\right)$ is the sorption capacity which can be determined experimentally, u [kg/kg$_s$] represents the material moisture content on dry basis, φ [%] is the inner relative humidity of the material, and ρ_s [kg/m^3] is the dry bulk density of the material.

Thus, the moisture balance equation (1) can be transformed in terms of relative humidity into:

$$\xi \frac{\partial \varphi}{\partial t} + \vec{\nabla} \cdot \left(-\xi \left(D_{l,\theta} + D_{v,\theta} \right) \vec{\nabla} \varphi \right) = 0 \tag{4}$$

3.1.2 Heat transfer

The energy conservation equation is given by:

$$\frac{\partial \hat{H}}{\partial t} + \vec{\nabla} \cdot \vec{q} = 0 \tag{5}$$

where $\hat{H}$ [J/m^3] is the total volumetric enthalpy and $\vec{q}$ [W/m²] is the heat flux which is transferred by thermal conduction, convection and phase change:

$$\hat{H} = \rho_s c_{p,s} \left(T - T_{ref}\right) + \rho_l c_{p,l} \left(T - T_{ref}\right) + \rho_v \left(L_v + c_{p,v} \left(T - T_{ref}\right)\right) \tag{6}$$

$$\vec{q} = -\lambda \vec{\nabla} T + \vec{g}_l c_{p,l} (T - T_{ref}) + \vec{g}_v c_{p,v} (T - T_{ref}) + \vec{g}_v L_v \tag{7}$$

where λ [W/(m.K)] is the thermal conductivity of the material, and $c_{p,s}$, $c_{p,l}$ and $c_{p,v}$ [J/(kg.K)] are the specific heats of dry material, liquid water and water vapour, respectively. T_{ref} = 273.15 K is the reference temperature, and L_v = 2.5 × 10^6 J/kg is the latent heat of vaporisation of water at the reference temperature T_{ref}.

Substituting Eq. (6-7) into Eq. (5), the energy conservation leads to an equation that depends on both temperature and moisture:

233 $$\rho_s c_{p,m}\frac{\partial T}{\partial t}+\vec{\nabla}\cdot\left(-\lambda\vec{\nabla}\mathrm{T}\right)+\vec{\nabla}\cdot\left(\xi\left(D_{l,\theta}c_{p,l}(T-T_{ref})+D_{v,\theta}\left(c_{p,v}\left(T-T_{ref}\right)+L_v\right)\right)\vec{\nabla}\varphi\right)$$
$$-\left(c_{p,l}(T-T_{ref})\frac{\partial\rho_l}{\partial t}+\left(c_{p,v}(T-T_{ref})+L_v\right)\frac{\partial\rho_v}{\partial t}\right)=0 \quad (8)$$

234 where $c_{p,m}$ [J/(kg.K)] is the heat capacity of the material, such that $c_{p,m}=c_{p,s}+\frac{\rho_v}{\rho_s}c_{p,v}+\frac{\rho_l}{\rho_s}c_{p,l}$.

235 3.2 Boundary conditions

236 Heat and mass transfers are applied to the upper surface, assuming that no transfer is
237 possible at the sides and at the bottom of the sample (see again Fig. 3). The moisture flow
238 through the surface $\dot{g}$ [kg/(m².s)] reads:

239 $$\dot{g}_{surf}=-\beta_m(P_v-P_{v,a}) \quad (9)$$

240 where β_m [kg/(Pa.m².s)] is the convective moisture transfer coefficient which can be
241 calculated using the convective heat transfer coefficient h_c [W/(m².K)] (Liu et al., 2015):
242 $\beta_m=7.7\times10^{-9}h_c$. In Eq. (9), P_v [Pa] represents the partial pressure of water vapour, which is
243 moisture-dependent so that $P_v=\varphi P_{v,sat}$, and $P_{v,surf}$ [Pa] is the ambient pressure above the
244 material surface.

245 The heat flow $\dot{q}$ [W/m^2] across the upper material surface involves convection and
246 radiation fluxes, and is given by:

247 $$\dot{q}_{surf}=-h_{surf}\left(T-T_a\right)+\left(L_v+c_{p,v}\left(T-T_{ref}\right)\right)\dot{g}_{surf} \quad (10)$$

248 where h_{surf} [W/(m².K)] is the global heat transfer coefficient which combines convection h_c
249 and radiation h_r such that $h_{surf}=h_c+h_r$. T_a [K] is the ambient temperature in the climatic
250 chamber.

4 Input properties

In order to feed the numerical model, several quantities need to be measured, such as sorption capacity and thermal conductivity. The other quantities that need to be known were found in the literature.

4.1 Isothermal sorption

A gravimetric method was applied for the measurement of the isothermal sorption curve according to ISO12571-2000[2], which consists in following the changes of mass of the material as a function of relative humidity. For that purpose, 6 cubic samples of side 35 mm were first dried at 60°C in a ventilated oven according to ASTM C1498-01[3]. Then, the dried samples were placed in the same climatic chamber as before at controlled relative humidity and fixed temperature of 23°C. The samples were weighed at regular intervals until the mass stabilised within less than 0.1%, so that the material was assumed to be at equilibrium. The tests were repeated and averaged for seven levels of relative humidity: 20, 30, 40, 50, 60, 70 and 80% RH, from which the sorption curve could be obtained. Because of the low water permeability of the sample, the whole experiment lasted for several weeks, depending on the considered RH. Reaching the equilibrium indeed takes much longer at high ambient relative humidity.

4.2 Thermal conductivity

The Hot Disk TPS 2500 S analyser (Fig. 5) was used to measure the thermal conductivity of the wood-cement material. The method is based on a transiently heated plane sensor that acts as both heat source and dynamic temperature probe. This sensor consists of an electrically conducting pattern in the shape of a double spiral, which has been etched out of a

[2] Hygrothermal performance of building materials and products: Determination of hygroscopic sorption properties, 2000

[3] Standard Test Method for Hygroscopic Sorption Isotherms of Building Materials, ASTM International, West Conshohocken, PA, 2001

thin nickel foil and sandwiched between two thin sheets of Kapton®. During the experiment, the hot disk sensor was fitted between two identical pieces of samples to be investigated, having relevant sizes (i.e., same as before: cubes of side 35 mm) for considering them as semi-infinite media with respect to sensor size. The thermal conductivity was calculated with the Hot Disk 6.1 software, based on tests carried out at equilibrium for different levels of relative humidity at fixed temperature of 23°C.

4.3 Moisture diffusivity

The moisture diffusivity D_θ characterises the moisture transfer ability through a material under a gradient of vapour pressure, and is such that $D_\theta = D_{l,\theta} + D_{v,\theta}$. The latter terms are the moisture diffusivities in liquid phase, $D_{l,\theta}$, and in vapour phase, $D_{v,\theta}$. Their values were taken from the literature (Bouguerra et al., 1999; Houngan et al., 2015) for a wood-cement composite and are presented in Fig. 6 as a function of moisture content. We indeed assumed that the behaviour of our material is similar to that reported in the literature, due to its very close composition, and this assumption was validated below by our parametric numerical study. As clearly seen in Fig. 6, the vapour diffusivity of wood-cement composite decreases when the water content increases, due to capillary condensation. On the contrary, the liquid diffusivity dramatically increases because of the high relative humidity at which the liquid water tends to saturation in the pores, which allows the water to be free and thus to diffuse more easily.

4.4 Other parameters and initial conditions

Other properties of wood-cement material, as well input parameters for the model, are listed in Table 3.

5 Results and discussion

5.1 Moisture sorption and related changes of thermal conductivity

Fig. 7 shows the water sorption curve of the wood-cement composite material between 20 % and 80 % RH, obtained from the procedure described in section 4.1, i.e., averaged on 6 different samples. The experimental data were correctly fitted by the Guggenheim – Anderson – de Boer (GAB) model, which has been widely used for fitting the moisture adsorption-desorption curve of bio-based building materials. It reads (Anderson, 1946; De Boer, 1953; Guggenheim, 1966):

$$u = \frac{X_G C_G K \varphi}{(1 - K\varphi)(1 + (C_G - 1)K\varphi)} \tag{11}$$

where X_G, C_G and K are adjustable parameters. For the material studied, X_G = 0.0359, C_G = 29.689 and K = 0.839 were found from the fit presented in Fig. 7.

The thermal conductivity λ measured at each hygrothermal equilibrium as described in section 4.2 is illustrated in Fig. 8, and was linearly fitted as a function of relative humidity: $\lambda = a\,\varphi + b$, where a and b are adjustable parameters. As expected, λ increases with relative humidity. All experimental results thus show the clear dependency of relative humidity on both hygric and thermal properties of wood-cement composite material, in complete agreement with the literature (Lelievre et al., 2014; Palumbo et al., 2016).

5.2 Model validation

The previous equations (4) and (8) describing the coupled heat and moisture transfers have been solved with the commercial software Comsol Multiphysics using the finite-element method. The model was first validated by the benchmark case in HAMSTAD project (Hagentoft et al., 2004), which is a platform for evaluating the numerical model of heat and moisture transfers for building walls. For the simulation of hygrothermal tests, 8820 triangle meshes were set. The mesh size, time step and tolerance were 2 mm, 30 s and 10^{-8},

319 respectively. The running time was less than 10 min. Experimental and simulation results of
320 the fast cycling test described in section 2.2 are compared in Fig. 9.
321 Experimental evolutions show cyclic variations of mass and temperature. The mass
322 variation shows increases then decreases. The increase in mass is due to the sudden increase
323 in the ambient relative humidity, and therefore the vapour pressure becomes greater than the
324 vapour pressure at the surface of the material, which has the effect of vapour flow to the
325 material and thereby increases its water content. Conversely, the decrease in mass is due to
326 the decrease in the relative humidity, which passes below its equilibrium value at the surface.
327 With regard to the temperature, during the mass gain, there is a rapid increase thereof,
328 then a slower decrease tending towards the equilibrium temperature. Conversely, these two
329 steps are also observable during the loss of mass. The first step (sudden increase in
330 temperature) is due to the condensation of the steam during the mass gain. This phenomenon
331 could be explained by the increase of the temperature of the chamber recorded by the sensor,
332 but a complementary simulation showed that this phenomenon also existed when the
333 temperature was fixed.
334 The second step observed, corresponding to a slow decrease in temperature, is explained
335 by a compensation of the mass flow towards the interior of the material. As the water content
336 increases at the surface, a water content gradient is created from the outside to the inside,
337 which imposes a flow of steam inwards. When this vapour leaves the volume concerned, there
338 is then a transfer of energy that compensates for the increase in temperature relative to the
339 superficial condensation. During the evaporation steps, these phenomena appear in the
340 opposite direction.
341 The measured and calculated amplitudes of both temperature and moisture are almost
342 identical, although some differences are observed. Indeed, it can be seen on the temperature
343 profile at 8 mm deep (Fig. 9a) that the difference between experiment and simulation is about

344 0.3°C for both adsorption and desorption phases. Besides, the results of temperature
345 simulation at 24 mm deep upon desorption are very close to the measurements, whereas a
346 deviation of 0.5°C can be observed upon adsorption (Fig. 9b). The temperature values at
347 different depths (8 and 24 mm) are very close to each other when simulated, but this is not the
348 same as for the experimental ones. It is possible that such differences originate from physical
349 phenomena not taken into account in the model. For instance, vapour diffusion associated to
350 temperature gradient was neglected in this study, and this may impact the changes of
351 temperature. Similar shifts between experimental and simulated temperature profiles can be
352 found in (Lelievre et al., 2014) for bio-based building materials.

353 On the mass profile (Fig. 9c) the difference between experiment and simulation is less
354 than 2%. The amplitude represents the amount of moisture adsorbed and desorbed by the
355 sample during the whole cycle. The simulation suggests that the cyclic changes are rather
356 constant, whereas the experimental recordings show a slight global increase with time, better
357 seen at day #9.

358 ## 5.3 Model sensitivity analysis

359 The numerical model developed herein allows predicting the hygrothermal transfers in
360 the porous medium. Nevertheless, several factors may have an impact on the simulation
361 results, so that parametric studies are required, focusing on boundary conditions (air
362 temperature and relative humidity) and moisture diffusion coefficients.

363 ### *5.3.1 Boundary conditions*

364 In order to check the effect of the boundary conditions on the temperature profiles, the air
365 temperature in the climatic chamber was varied, and its impact on the simulation results is
366 illustrated in Fig. 10a and 10b. The results were only shown up to 4 days for clarity. At fixed
367 relative humidity, no influence was found on both position and amplitude of each peak when

368 the air temperature varied by ± 0.5 °C. The variation of air temperature caused a deviation of
369 ± 3 % of the temperatures inside the material, but no change of mass.

370 In contrast, the variation of relative humidity of air by ± 5% at fixed temperature had a
371 significant impact on the mass, as evidenced in Fig. 10c. In this figure, the temperature was
372 not shown since it did not change. The position and amplitude of mass at each peak also
373 remained almost constant, but the increase or decrease of RH in air tended to increase or
374 reduce the mass, respectively. Therefore, the change of RH has a significant effect on the
375 moisture transfer in the material. This finding demonstrates that monitoring very accurately
376 the environment in the climatic chamber is necessary for obtaining reliable results.

377 *5.3.2 Moisture diffusivity*

378 The impact of moisture diffusivity in vapour and liquid phase on the prediction of
379 hygrothermal transfer was evaluated by varying the values of $D_{v,\theta}$ and $D_{l,\theta}$, respectively, by ±
380 25 %. As shown in Fig. 11, increasing the two moisture diffusion coefficients (referred to as
381 $D_\theta \times 1.25$ in the plots) led to the increase of both the inner relative humidity and the mass of
382 the sample. The difference of mass change was about 0.3%. Reciprocally, the reduction of
383 moisture diffusion coefficients (referred to as $D_\theta \times 0.75$) caused a decrease of both the inner
384 relative humidity and the mass of the sample. However, the three temperature profiles were
385 very close to each other. The simulation thus proves that the moisture diffusion coefficients
386 have a low influence on the results obtained.

387 5.4 Moisture buffering value

388 The moisture buffering value, MBV [g/(m^2.%RH)], quantifies the ability of a given
389 building material to adsorb and release moisture. This is an important parameter with respect
390 to interior comfort. It is calculated by (Rode, 2005):

391 $$MBV = \frac{\Delta m}{A \cdot \left(RH_{high} - RH_{low} \right)} \quad (12)$$

where Δm [g] is the variation of mass during moisture adsorption and release, A [m²] is the contact area of the sample with air, and RH_{high} and RH_{low} [%] represent high and low relative humidity (75% and 33%, respectively). The mass change experimentally measured during 24h is presented in Fig. 12.

The MBV are classified according to Fig. 13. The highest values correspond to building materials that best allow regulating the indoor relative humidity, and which are thus referred to as “excellent” from this point of view. The MBV of the present wood-cement composite material was found to be 1.16 g/(m².%RH), and hence can be considered as "good" (i.e., 1 < MBV < 2). This finding confirms that this building material can contribute to the improvement of the indoor hygrothermal comfort.

6 Conclusion

A wood-cement composite material based on recycled wood waste was investigated in terms of hygrothermal transfers, with an expected impact on the indoor comfort.

Heat and moisture transfers in such porous medium were described by mass and energy balance equations, and hygrothermal properties were also determined experimentally with relative humidity dependence and then used as input parameters for the numerical model.

The simulations results were found to be in good agreement with the experiments, thereby confirming the relevance of the used material properties. However, slight differences between experiments and simulations were observed, which might originate from physical phenomena not considered in the model (such as vapour diffusion associated with temperature gradient).

Sensitivity analysis on the boundary conditions such as temperature or relative humidity of air had a non-negligible impact on the results. Moreover, the moisture diffusion coefficients had a slight impact on the moisture transfer. A good moisture buffering capacity

was found that confirms the potential of the present wood-cement composite for regulating the indoor humidity.

The present paper is a first step towards in-depth studies of the hygrothermal behaviour of wood-cement composites from material scale to building scale. The properties measured herein and the model that was developed can indeed be applied for studying heat and moisture transfers in buildings incorporating this type of formwork, so that its benefit can be firmly established. Moreover, the study of thickness impact could be interesting for future development.

References

Akkaoui, A., 2014. Béton de granulats de bois: Etude expérimentale et théorique des propriétés thermo-hydro-mécaniques par des approches multi-échelles (Ph.D thesis). Université Paris-Est.

Akkaoui, A., Caré, S., Vandamme, M., 2017. Experimental and micromechanical analysis of the elastic properties of wood-aggregate concrete. Constr. Build. Mater. 134, 346–357. https://doi.org/10.1016/j.conbuildmat.2016.12.084

Anderson, R.B., 1946. Modifications of the Brunauer, Emmett and Teller Equation. J. Am. Chem. Soc. 68, 686–691. https://doi.org/10.1021/ja01208a049

Bouguerra, A., Sallée, H., De Barquin, F., Dheilly, R.M., Quéneudec, M., 1999. Isothermal moisture properties of wood-cementitious composites. Cem. Concr. Res. 29, 339–347. https://doi.org/10.1016/S0008-8846(98)00232-4

Boutin, M.P., Flamin, C., Quinton, S., Gosse, G., 2006. Étude des caractéristiques environnementales du chanvre par l'analyse de son cycle de vie | Alim'agri.

Campbell, M.D., Coutts, R.S.P., 1980. Wood fibre-reinforced cement composites. J. Mater. Sci. 15, 1962–1970. https://doi.org/10.1007/BF00550621

Cetiner, I., Shea, A.D., 2018. Wood waste as an alternative thermal insulation for buildings. Energy Build. 168, 374–384. https://doi.org/10.1016/j.enbuild.2018.03.019

Cheah, C.B., Ramli, M., 2011. The implementation of wood waste ash as a partial cement replacement material in the production of structural grade concrete and mortar: An overview. Resour. Conserv. Recycl. 55, 669–685. https://doi.org/10.1016/j.resconrec.2011.02.002

Chowdhury, S., Maniar, A., Suganya, O.M., 2015. Strength development in concrete with wood ash blended cement and use of soft computing models to predict strength parameters. J. Adv. Res. 6, 907–913. https://doi.org/10.1016/j.jare.2014.08.006

Colinart, T., Glouannec, P., 2017. Temperature dependence of sorption isotherm of hygroscopic building materials. Part 1: Experimental evidence and modeling. Energy Build. 139, 360–370. https://doi.org/10.1016/j.enbuild.2016.12.082

De Boer, J.H., 1953. The dynamical character of adsorption. Oxf. Univ. Press.

Dhakal, U., Berardi, U., Gorgolewski, M., Richman, R., 2017. Hygrothermal performance of hempcrete for Ontario (Canada) buildings. J. Clean. Prod. 142, Part 4, 3655–3664. https://doi.org/10.1016/j.jclepro.2016.10.102

456 Evrard, A., deHerd, A., 2010. Hygrothermal performance of lime-hemp wall assemblies. J.
457 Build. Phys. 34, 5–25. https://doi.org/10.1177/1744259109355730
458 Guggenheim, E., 1966. Application of statistical mechanics. Oxf. Univ. Press.
459 Hagentoft, C.-E., Kalagasidis, A.S., Adl-Zarrabi, B., Roels, S., Carmeliet, J., Hens, H.,
460 Grunewald, J., Funk, M., Becker, R., Shamir, D., Adan, O., Brocken, H., Kumaran, K.,
461 Djebbar, R., 2004. Assessment method of numerical prediction models for combined
462 heat, air and moisture Transfer in building components: benchmarks for one-
463 dimensional cases. J. Therm. Envel. Build. Sci. 27, 327–352.
464 https://doi.org/10.1177/1097196304042436
465 Hameury, S., Lundström, T., 2004. Contribution of indoor exposed massive wood to a good
466 indoor climate: in situ measurement campaign. Energy Build. 36, 281–292.
467 https://doi.org/10.1016/j.enbuild.2003.12.003
468 Helsen, L., Van den Bulck, E., 2005. Review of disposal technologies for chromated copper
469 arsenate (CCA) treated wood waste, with detailed analyses of thermochemical
470 conversion processes. Environ. Pollut. 134, 301–314.
471 https://doi.org/10.1016/j.envpol.2004.07.025
472 Houngan, A.C., Awanto, C., Fagbemi, L., Anjorin, M., Vianou, A., 2015. Mass diffusivity
473 measurements of two cement based materials. J. Civ. Eng. Constr. Technol. 6, 86–92.
474 Incropera, F.P., Dewitt, D.P., Bergman, T.L., Lavine, A.S., 2006. Fundamentals of heat and
475 mass transfer, 6th ed. John Wiley and Sons Inc.
476 Karade, S.R., 2010. Cement-bonded composites from lignocellulosic wastes. Constr. Build.
477 Mater. 24, 1323–1330. https://doi.org/10.1016/j.conbuildmat.2010.02.003
478 Kim, M.H., Song, H.B., 2014. Analysis of the global warming potential for wood waste
479 recycling systems. J. Clean. Prod. 69, 199–207.
480 Kunzel, H.M., 1995. Simultaneous heat and moisture transport in building components: one-
481 and two-dimensional calculation using simple parameters. Fraunhofer IRB Verl.
482 Suttgart ISBN 3-8167-4103-7.
483 Lelievre, D., Colinart, T., Glouannec, P., 2014. Hygrothermal behavior of bio-based building
484 materials including hysteresis effects: Experimental and numerical analyses. Energy
485 Build. 84, 617–627. https://doi.org/10.1016/j.enbuild.2014.09.013
486 Li, M., Khelifa, M., El Ganaoui, M., 2017. Mechanical characterization of concrete
487 containing wood shavings as aggregates. Int. J. Sustain. Built Environ. 6, 587–596.
488 https://doi.org/10.1016/j.ijsbe.2017.12.005
489 Li, M., Khelifa, M., Khennane, A., El Ganaoui, M., 2019. Structural response of cement-
490 bonded wood composite panels as permanent formwork. Compos. Struct. 209, 13–22.
491 https://doi.org/10.1016/j.compstruct.2018.10.079
492 Li, M., Khennane, A., Brandelet, B., El Ganaoui, M., Khelifa, M., Rogaume, Y., 2018.
493 Modelling of heat transfer through permanent formwork panels exposed to high
494 temperatures. Constr. Build. Mater. 185, 166–174.
495 https://doi.org/10.1016/j.conbuildmat.2018.07.052
496 Liu, X., Chen, Y., Ge, H., Fazio, P., Chen, G., Guo, X., 2015. Determination of optimum
497 insulation thickness for building walls with moisture transfer in hot summer and cold
498 winter zone of China. Energy Build. 109, 361–368.
499 https://doi.org/10.1016/j.enbuild.2015.10.021
500 Lo, C.-L., 2017. Environmental benefits of renewable building materials: A case study in
501 Taiwan. Energy Build. 140, 236–244. https://doi.org/10.1016/j.enbuild.2017.02.010
502 López, O., Torres, I., Guimarães, A.S., Delgado, J.M.P.Q., de Freitas, V.P., 2017. Inter-
503 laboratory variability results of porous building materials hygrothermal properties.
504 Constr. Build. Mater. 156, 412–423.
505 https://doi.org/10.1016/j.conbuildmat.2017.08.184

Luikov, A.V., 1966. Heat and mass transfer in capillary-porous bodies. Pergamon, pp. 233–303.

Page, J., Khadraoui, F., Boutouil, M., Gomina, M., 2017. Multi-physical properties of a structural concrete incorporating short flax fibers. Constr. Build. Mater. 140, 344–353. https://doi.org/10.1016/j.conbuildmat.2017.02.124

Palumbo, M., Lacasta, A.M., Holcroft, N., Shea, A., Walker, P., 2016. Determination of hygrothermal parameters of experimental and commercial bio-based insulation materials. Constr. Build. Mater. 124, 269–275. https://doi.org/10.1016/j.conbuildmat.2016.07.106

Park, J.H., Kang, Y., Lee, J., Wi, S., Chang, J.D., Kim, S., 2019. Analysis of walls of functional gypsum board added with porous material and phase change material to improve hygrothermal performance. Energy Build. 183, 803–816. https://doi.org/10.1016/j.enbuild.2018.11.023

Pervaiz, M., Sain, M.M., 2003. Carbon storage potential in natural fiber composites. Resour. Conserv. Recycl. 39, 325–340. https://doi.org/10.1016/S0921-3449(02)00173-8

Qin, M., Belarbi, R., Aït-Mokhtar, A., Nilsson, L.-O., 2009. Coupled heat and moisture transfer in multi-layer building materials. Constr. Build. Mater. 23, 967–975. https://doi.org/10.1016/j.conbuildmat.2008.05.015

Qin, M., Zhang, H., 2015. Analytical methods to calculate combined heat and moisture transfer in porous building materials under different boundary conditions. Sci. Technol. Built Environ. 21, 993–1001. https://doi.org/10.1080/23744731.2015.1051464

Rahim, M., Douzane, O., Tran Le, A.D., Promis, G., Laidoudi, B., Crigny, A., Dupre, B., Langlet, T., 2015. Characterization of flax lime and hemp lime concretes: Hygric properties and moisture buffer capacity. Energy Build. 88, 91–99. https://doi.org/10.1016/j.enbuild.2014.11.043

Rode, C., 2005. Moisture buffering of building materials. Technical University of Denmark, Department of Civil Engineering. BYG Report, No. R-126 https://orbit.dtu.dk/files/2415500/byg-r126.pdf.

Sudin, R., Swamy, N., 2006. Bamboo and wood fibre cement composites for sustainable infrastructure regeneration. J. Mater. Sci. 41, 6917–6924. https://doi.org/10.1007/s10853-006-0224-3

Tran Le, A.D., Maalouf, C., Mai, T.H., Wurtz, E., Collet, F., 2010. Transient hygrothermal behaviour of a hemp concrete building envelope. Energy Build. 42, 1797–1806. https://doi.org/10.1016/j.enbuild.2010.05.016

Wang, L., Chen, S.S., Tsang, D.C.W., Poon, C.S., Shih, K., 2016a. Value-added recycling of construction waste wood into noise and thermal insulating cement-bonded particleboards. Constr. Build. Mater. 125, 316–325. https://doi.org/10.1016/j.conbuildmat.2016.08.053

Wang, L., Chen, S.S., Tsang, D.C.W., Poon, C.-S., Shih, K., 2016b. Recycling contaminated wood into eco-friendly particleboard using green cement and carbon dioxide curing. J. Clean. Prod. 137, 861–870. https://doi.org/10.1016/j.jclepro.2016.07.180

Wang, L., Ge, H., 2018. Stochastic modelling of hygrothermal performance of highly insulated wood framed walls. Build. Environ. 146, 12–28. https://doi.org/10.1016/j.buildenv.2018.09.032

Yoo, J., Chang, S.J., Lee, J., Wi, S., Kim, S., 2019. Numerical analysis of hygrothermal properties and behavior of Korean based cross-laminated timber (CLT) wall system to deduce optimal assemblies. J. Clean. Prod. 213, 1217–1227. https://doi.org/10.1016/j.jclepro.2018.12.221

556 Table 1. Mechanical properties of wood-cement panel (Li et al., 2018).

557

Wood-cement panel	Value (MPa)
Elastic modulus	1820
Elastic limit	1.6
Flexural strength	2.5
Compressive strength	5.3

558

559

560 Table 2. Composition of wood-cement composite material.

Ingredients	Wt. %	Vol. %
Wood	43.2	67.3
Cement	35.1	22.9
Silica	12.6	3.0
Water	9.1	6.8

561

562

563 Table 3. Input parameters and initial conditions

Parameter	Unit	Value	Ref
Specific heat of dry material $c_{p,s}$	J/(kg.K)	870	(Incropera et al., 2006)
Specific heat of liquid water $c_{p,l}$	J/(kg.K)	4180	(Incropera et al., 2006)
Specific heat of water vapour $c_{p,v}$	J/(kg.K)	1580	(Incropera et al., 2006)
Saturated water vapour pressure $P_{v,sat}$	Pa	$101325\times10^{\left(17.443-\frac{2795}{T}-3.868\times\log_{10}T\right)}$	(Incropera et al., 2006)
Latent heat of vaporization L_v	J/kg	2.5×10^{6}	(Incropera et al., 2006)
Global heat transfer coefficient h_{surf}	W/(m².K)	15	
Initial temperature T_0	°C	23.3	
Initial relative humidity φ_0	%	53	

564

Figure Caption

Fig. 1. Description of stay-in-place wood-cement formwork system: (a) photo of a construction site using wood-cement formwork; and (b) scheme of formwork system.

Fig. 2. (a) Raw bio-aggregate (spruce shavings); and (b) final wood-cement composite material.

Fig. 3. Experimental device for measuring temperature and mass changes: (a) scheme of sample cross-section with insulation and protection from moisture, and position of temperature probes; (b) and (c) sample with thermocouples, installed on an electronic balance in the climatic chamber, and connected to a computer.

Fig. 4. Dynamic conditions of ambiance temperature (T_a) and relative humidity (φ_a) measured in the climatic chamber during the test.

Fig. 5. Hot Disk device: (a) analyser; and (b) sensor with one sample.

Fig. 6. Moisture diffusivity in liquid phase, $D_{l,\theta}$, and in vapour phase, $D_{v,\theta}$, of wood-concrete material.

Fig. 7. Moisture sorption isotherm (red points) and its fit by the GAB equation (Eq. 11, black curve) such that $u = \frac{0.894\varphi}{(1-0.839\varphi)(1+24.07\varphi)}$.

Fig. 8. Measured thermal conductivity at 23°C as a function of relative humidity (black points), and its linear fit (red line) such that $\lambda = 0.0189\,\varphi + 0.1987$.

Fig. 9. Comparison between experimental (black dotted lines) and simulation (red continuous line) results during the fast cycling test: changes of temperature with time at (a) 8mm-deep; and (b) 24mm-deep; and (c) temporal changes of moisture.

Fig. 10. Experimental (black solid line) and simulated (dotted line) temperature evolutions with a variation of ± 0.5°C (reference in green, +0.5°C in blue, and -0.5°C in red): (a) at 8 mm deep, and (b) at 24 mm deep; (c) Simulated mass sample evolution with a variation of ± 5% on φ_a (with the reference in solid black line, +5% in dotted blue line, and -5% in dashed red line).

Fig. 11. Impact of moisture diffusivity on: (a) the inner relative humidity of the sample at 8 mm and 24 mm deep; and (b) the sample mass (red line: reference diffusion coefficients; blue

line: diffusion coefficients decreased by 25%; green line: diffusion coefficients increased by 25%).

Fig. 12. Change of mass of wood-cement composite during a fast cycling test repeated during at least 9 days at a fixed temperature (23°C) and high RH (75%) during 8 hours followed by low RH (33 %) during 16 hours.

Fig. 13. Practical MBV classification.

Modelling the hygrothermal behaviour of cement-bonded wood composite panels as permanent formwork

Figure 1

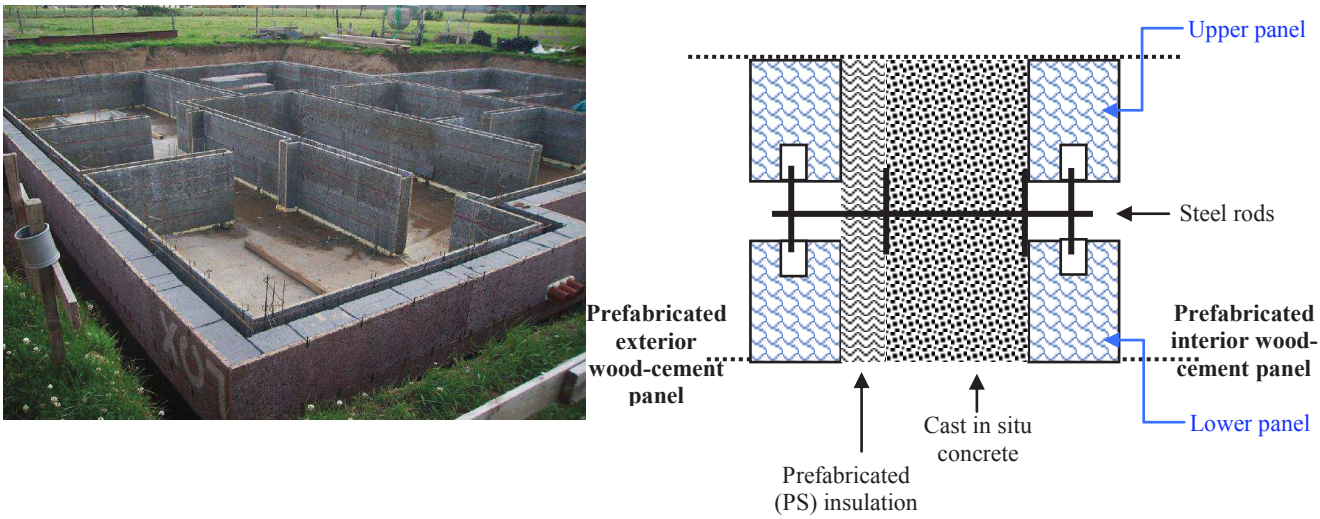

Modelling the hygrothermal behaviour of cement-bonded wood composite panels as permanent formwork

Figure 2

(a)

(b)

Modelling the hygrothermal behaviour of cement-bonded wood composite panels as permanent formwork

Figure 3

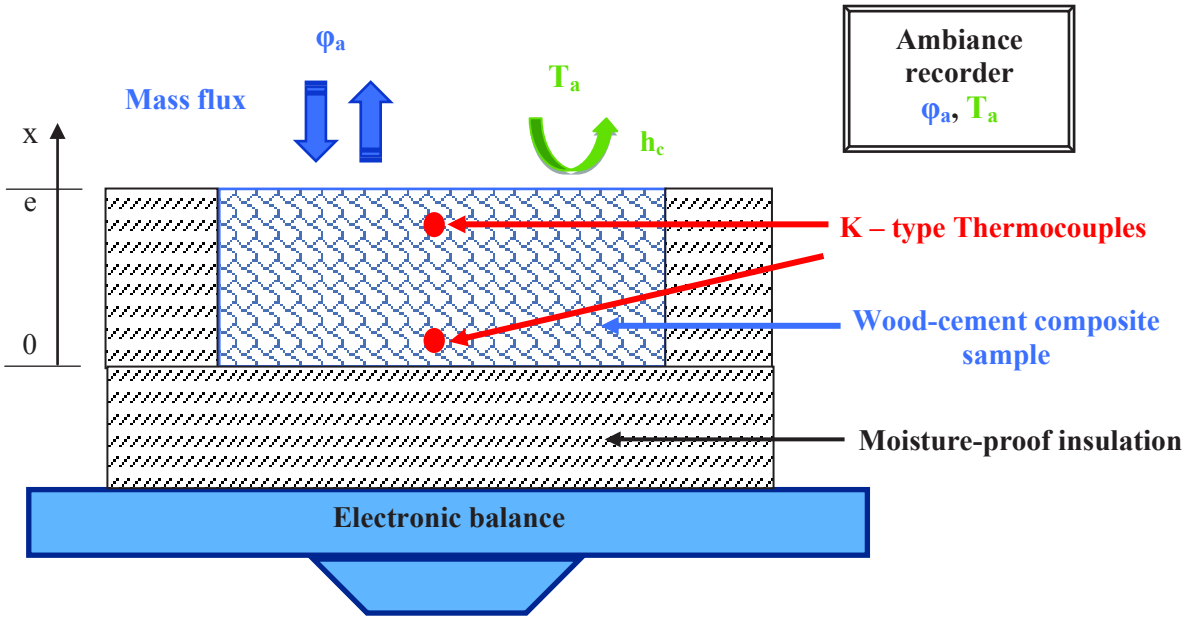

(a)

(b)

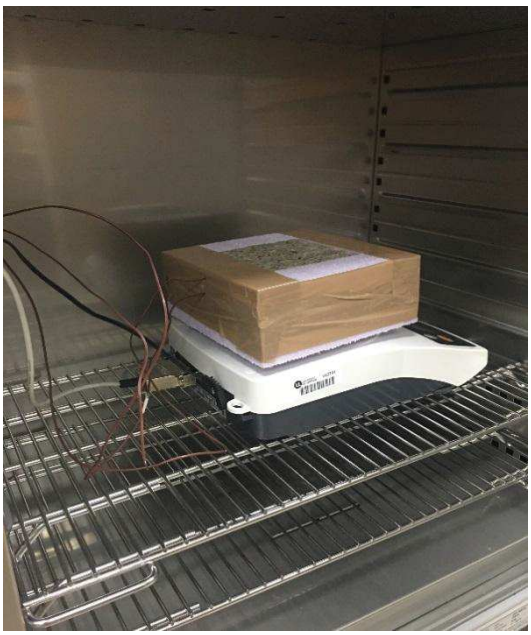

(c)

Modelling the hygrothermal behaviour of cement-bonded wood composite panels as permanent formwork

Figure 4

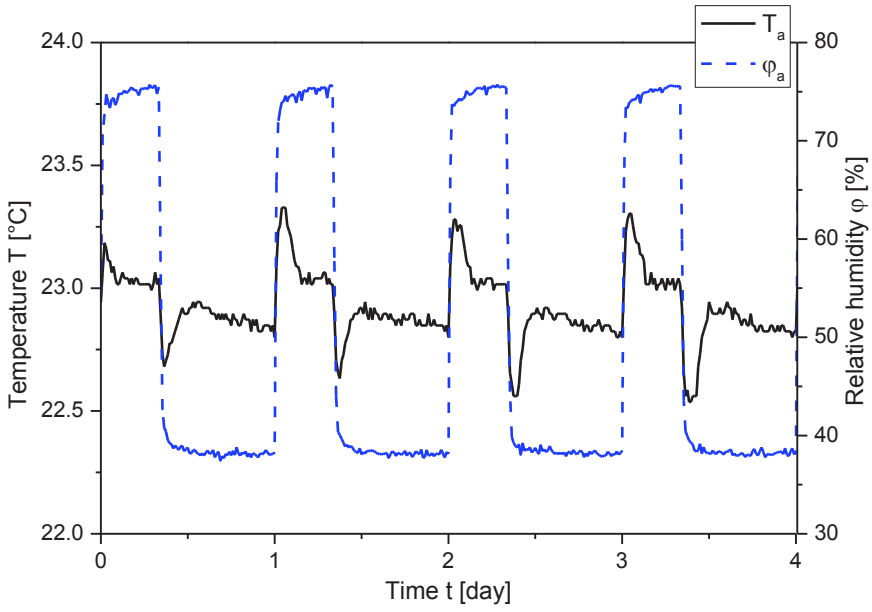

Modelling the hygrothermal behaviour of cement-bonded wood composite panels as permanent formwork

Figure 5

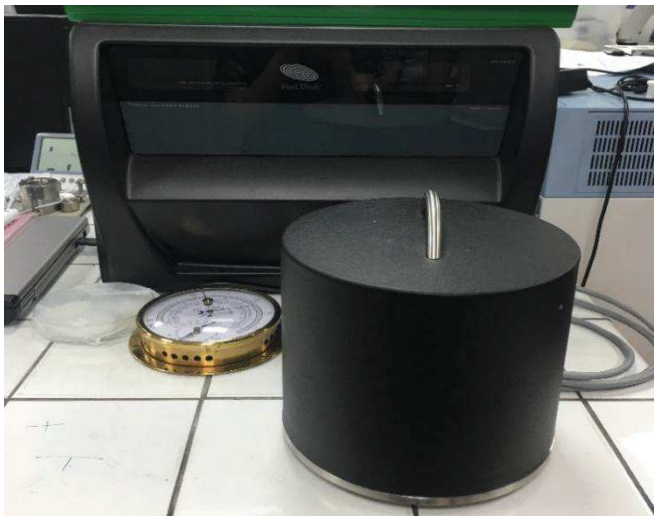

(a)

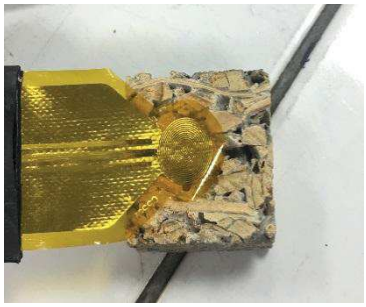

(b)

Modelling the hygrothermal behaviour of cement-bonded wood composite panels as permanent formwork

Figure 6

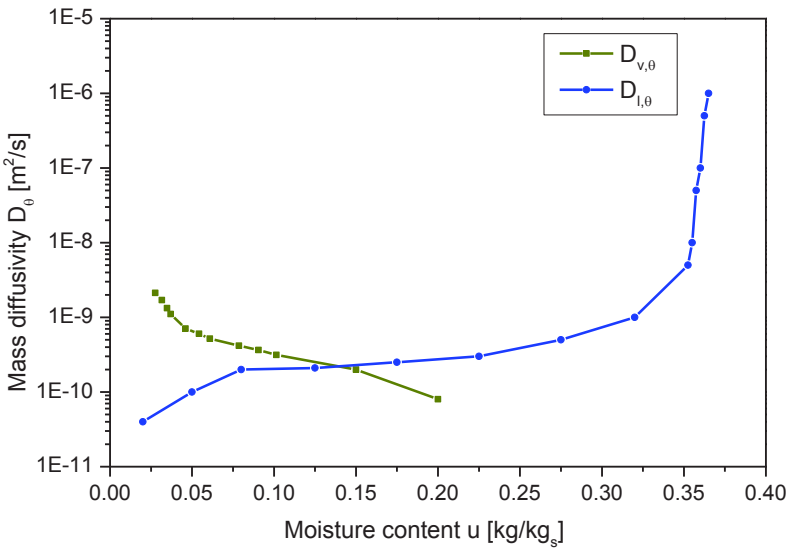

Modelling the hygrothermal behaviour of cement-bonded wood composite panels as permanent formwork

Figure 7

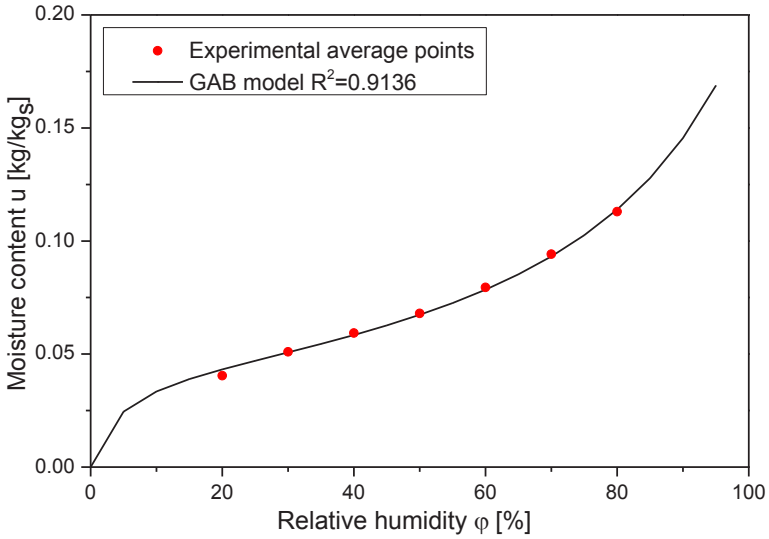

Modelling the hygrothermal behaviour of cement-bonded wood composite panels as permanent formwork

Figure 8

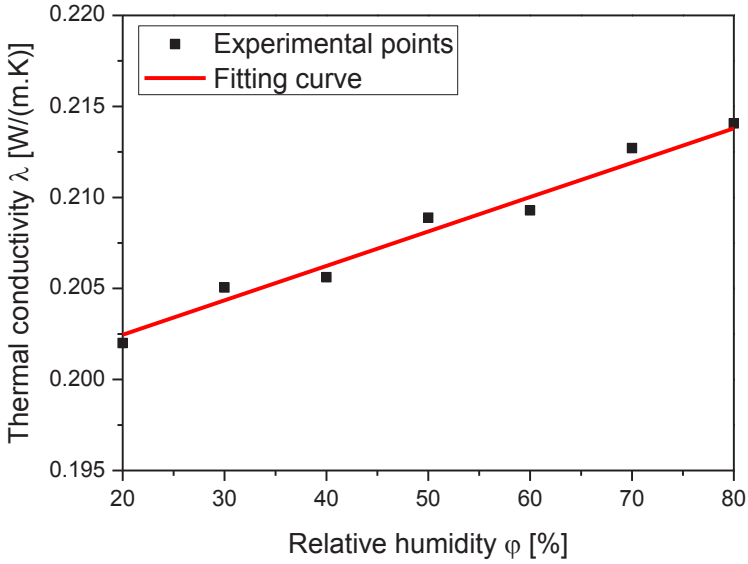

Modelling the hygrothermal behaviour of cement-bonded wood composite panels as permanent formwork

Figure 9

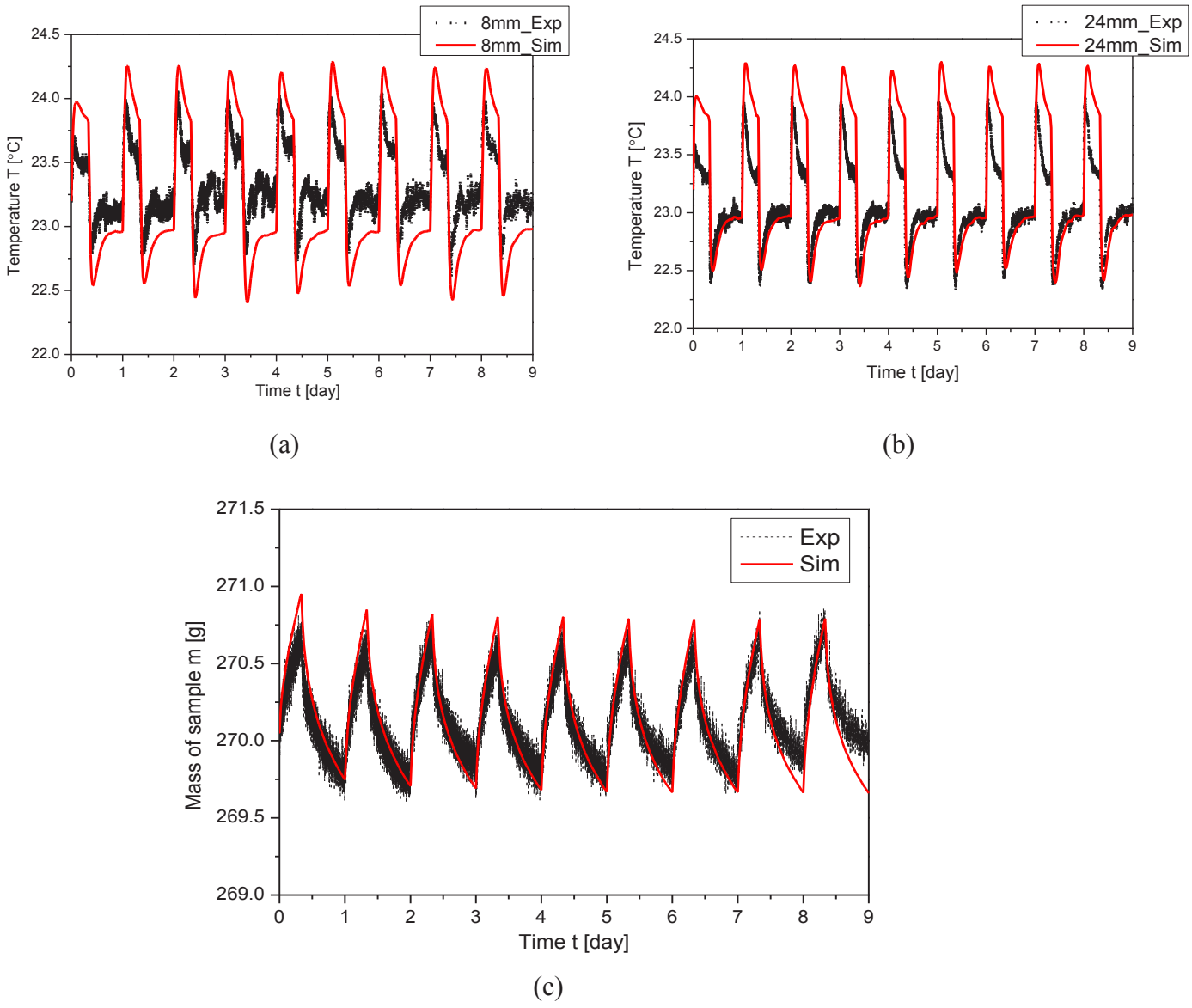

Modelling the hygrothermal behaviour of cement-bonded wood composite panels as permanent formwork

Figure 10

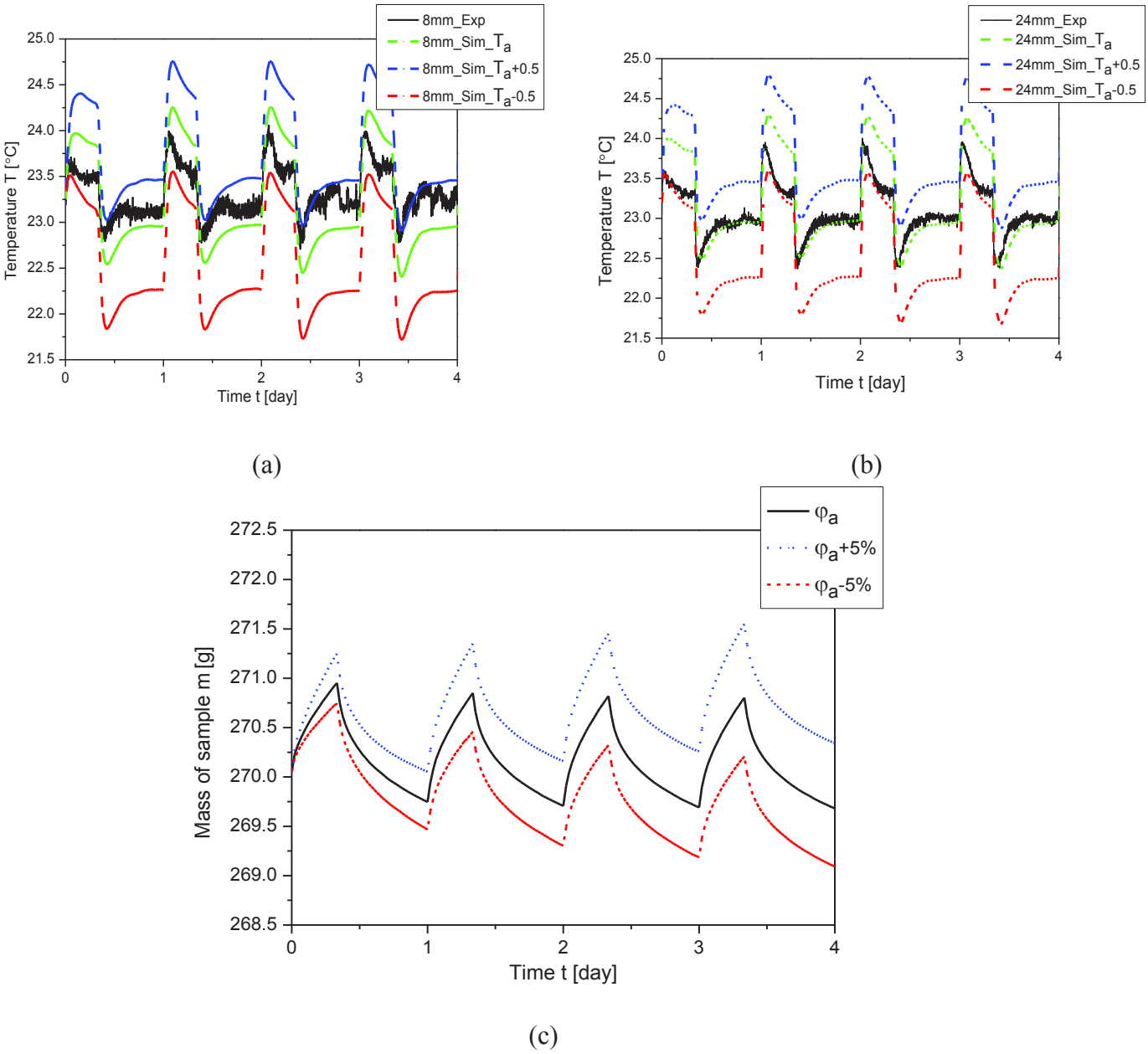

Modelling the hygrothermal behaviour of cement-bonded wood composite panels as permanent formwork

Figure 11

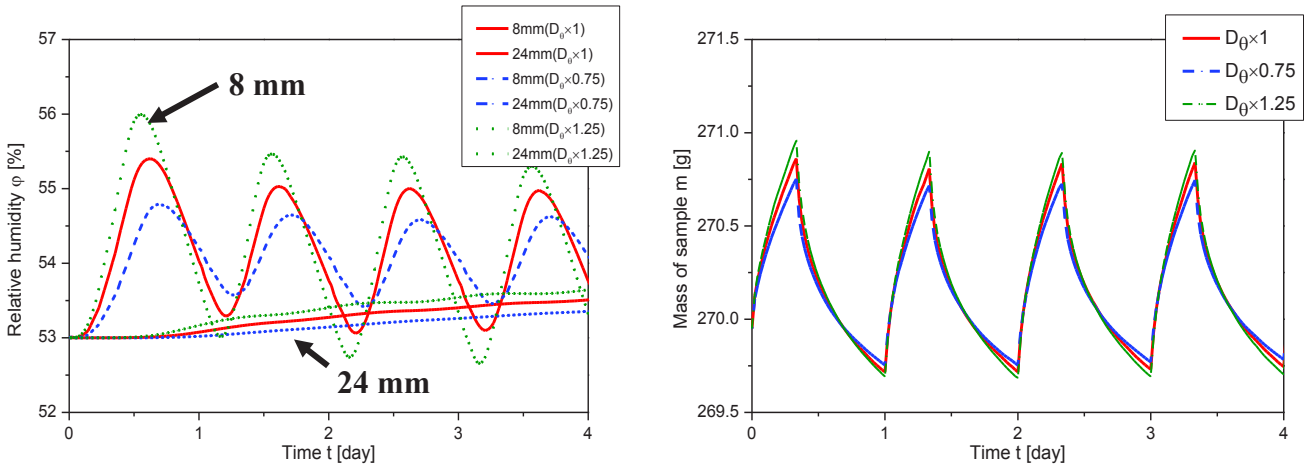

(a) (b)

Modelling the hygrothermal behaviour of cement-bonded wood composite panels as permanent formwork

Figure 12

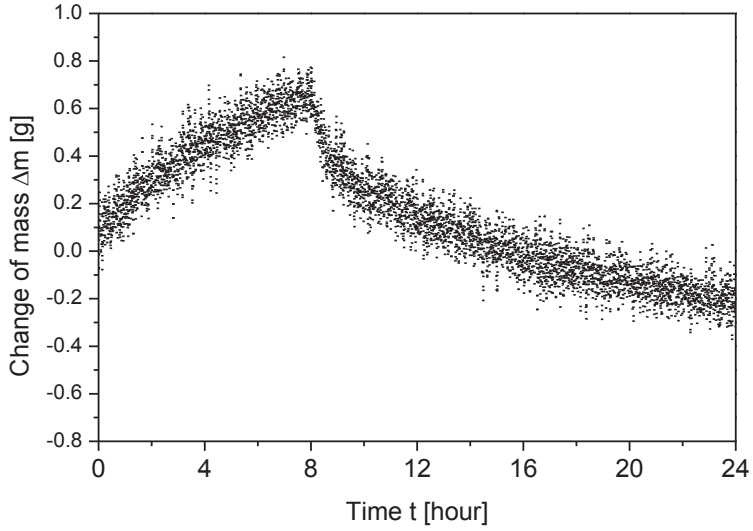

Modelling the hygrothermal behaviour of cement-bonded wood composite panels as permanent formwork

Figure 13